A&A 523, A88 (2010)
DOI: 10.1051/0004-6361/201014909

Astronomy & Astrophysics

The SOPHIE search for northern extrasolar planets

III. A Jupiter-mass companion around HD 109246⋆,⋆⋆

I. Boisse[1], A. Eggenberger[2], N. C. Santos[3], C. Lovis[4], F. Bouchy[1,5], G. Hébrard[1], L. Arnold[5], X. Bonfils[2,4], X. Delfosse[2], M. Desort[2], R. F. Díaz[1], D. Ehrenreich[2], T. Forveille[2], A. Gallenne[6], A. M. Lagrange[2], C. Moutou[7], S. Udry[4], F. Pepe[4], C. Perrier[2], S. Perruchot[5], F. Pont[8], D. Queloz[4], A. Santerne[7], D. Ségransan[4], and A. Vidal-Madjar[1]

[1] Institut d'Astrophysique de Paris, UMR7095 CNRS, Université Pierre & Marie Curie, 98bis Bd Arago, 75014 Paris, France
e-mail: iboisse@iap.fr
[2] Université Joseph Fourier – Grenoble 1 / CNRS, Laboratoire d'Astrophysique de Grenoble (UMR 5571), BP 53, 38041 Grenoble Cedex 9, France
[3] Centro de Astrofísica, Universidade do Porto, Rua das Estrelas, 4150-762 Porto, Portugal
[4] Observatoire de Genève, Université de Genève, 51 Ch. des Maillettes, 1290 Sauverny, Switzerland
[5] Observatoire de Haute Provence, CNRS/OAMP, 04870 Saint-Michel l'Observatoire, France
[6] European Southern Observatory, Casilla 19001, Santiago 19, Chile
[7] Laboratoire d'Astrophysique de Marseille, Université de Provence & CNRS, 38 rue Frédéric Joliot-Curie, 13388 Marseille cedex 13, France
[8] School of Physics, University of Exeter, Exeter EX4 4QL, UK

Received 30 April 2010 / Accepted 24 June 2010

ABSTRACT

We report the detection of a Jupiter-mass planet discovered with the SOPHIE spectrograph mounted on the 1.93-m telescope at the Haute-Provence Observatory. The new planet orbits HD 109246, a G0V star slightly more metallic than the Sun. HD 109246b has a minimum mass of 0.77 $M_{\rm Jup}$, an orbital period of 68 days, and an eccentricity of 0.12. It is placed in a sparsely populated region of the period distribution of extrasolar planets. We also present a correction method for the so-called seeing effect that affects the SOPHIE radial velocities. We complement this discovery announcement with a description of some calibrations that are implemented in the SOPHIE automatic reduction pipeline. These calibrations allow the derivation of the photon-noise radial velocity uncertainty and some useful stellar properties ($v \sin i$, [Fe/H], $\log R'_{\rm HK}$) directly from the SOPHIE data.

Key words. planetary systems – techniques: radial velocities – stars: individual: HD 109246 – stars: activity – stars: abundances

1. Introduction

Fifteen years after the first discovery of a planet orbiting another solar-type star (Mayor & Queloz 1995), about 450 extrasolar planets have been announced. Most of them were detected with the same historical technique: high-precision radial velocimetry. Although several methods now allow routine detection of extrasolar planets, high-precision radial velocimetry will remain at the forefront of exoplanet science in the coming years. Indeed, thanks to continuous efforts to improve the instrumental sensitivity (e.g. Mayor et al. 2009) and to overcome the limitation of stellar activity (e.g. Udry et al. 2006), radial velocimetry is a particularly efficient technique for detecting low-mass planets (e.g. Mayor et al. 2009). Furthermore, radial-velocity (RV) measurements are needed to establish the true nature of transiting planetary candidates, to derive their mass, and to measure spin-orbit alignment angles via the Rossiter-MacLaughlin effect (e.g. Queloz et al. 2000; Ohta et al. 2005; Winn 2010; Triaud et al. 2010). The numerous projects of future high-resolution spectrographs operating either at infrared (SPIRou, UPF, SIMPLE) or at visible wavelengths (ESPRESSO, CODEX) denote the field development and illustrate the importance of RV measurements in exoplanetary science.

The high-precision SOPHIE spectrograph (Perruchot et al. 2008; Bouchy et al. 2009b) has replaced ELODIE (Baranne et al. 1996; Queloz et al. 1998b) at the Cassegrain focus of the 1.93-m telescope at the Haute-Provence Observatory (OHP, France). Opened to the community since October 2006, SOPHIE has led to many discoveries in various research fields, including the follow-up of transiting planet candidates from the SuperWASP (e.g. Cameron et al. 2007), HAT (Bakos et al. 2007), and CoRoT (e.g. Bouchy et al. 2008) surveys; asteroseismology (Mosser et al. 2008); and the dynamics of binary stars (Albrecht et al. 2009). In late-2006, the SOPHIE consortium initiated a large program to search for and characterize extrasolar planets (Bouchy et al. 2009b). This comprehensive survey is both a continuation and an extension of the planet-search programs carried out with the ELODIE spectrograph (e.g. Mayor & Queloz 1995; Delfosse et al. 1998; Perrier et al. 2003; Galland et al. 2005; Naef et al. 2005; Da Silva et al. 2006).

HD 109246 was observed as part of the second subprogram from the SOPHIE consortium. This subprogram comprises two parts: a survey for giant planets in a volume-limited sample of ~2000 FGK dwarfs, and a follow-up of known transiting giant

⋆ Based on observations made with the SOPHIE spectrograph on the 1.93-m telescope at Observatoire de Haute-Provence (CNRS/OAMP), France (program 07A.PNP.CONS).

⋆⋆ RV tables (Tables C.1 and C.2) are only available in electronic form at the CDS via anonymous ftp to cdsarc.u-strasbg.fr (130.79.128.5) or via http://cdsarc.u-strasbg.fr/viz-bin/qcat?J/A+A/523/A88

planets (Bouchy et al. 2009b). Previous discoveries from the main survey include the detection of both a massive planet (or light brown dwarf) around HD 16760 (Bouchy et al. 2009b) and of a two-planet system around HD 9446 (Hébrard et al. 2009). The follow-up part allowed the observation of the spectroscopic transits (Rossiter-McLaughlin effect) of three planets and revealed the two first cases of spin-orbit misalignement (Loeillet et al. 2008; Hébrard et al. 2008; Moutou et al. 2009; Pont et al. 2009; Hébrard et al. 2010).

Here, we report the discovery of a Jupiter-mass planet orbiting HD 109246. The observations are presented in Sect. 2 and the characteristics of the host star are described in Sect. 3. In Sect. 4 we derive the best-fit Keplerian model to the velocities of HD 109246 and correct for an instrumental effect on radial velocities due to seeing variation. We summarize and discuss our results in Sect. 5. In the Appendices, we describe the calibrations implemented in the SOPHIE automatic reduction pipeline to derive the photon-noise RV uncertainty (A), the projected rotational velocity $v \sin i$ (B.1), the metallicity index [Fe/H] (B.2), and the activity index $\log R'_{\rm HK}$ (C).

2. Radial-velocity measurements

We observed HD 109246 with the SOPHIE spectrograph from January 2007 to February 2010. The measurements were performed in high-resolution mode (resolution power of $\Delta\lambda/\lambda \approx 75\,000$) and at constant signal-to-noise ratio (*SNR*) (*SNR* variations $\sigma_{SNR} \simeq 8\%$). Exposure times ranged from 270 to 1200 s, following the variations of seeing and sky transparency at OHP. We used the objAB observing mode with one of SOPHIE's fiber recording the starlight and the other fiber observing the sky to estimate the background contamination (e.g. moonlight). Both fibers were fed with a Thorium-Argon lamp every ~2 h for wavelength calibration. SOPHIE is environmentally stabilized and the intrinsic drift of the spectrograph (mainly because of small variations of pressure and temperature) is less than 3 m s^{-1} per hour. Each exposure was corrected for the instrumental drift by interpolating the measured intrinsic drift over the ~2 h period. This method allows a precision of ~2 m s^{-1} on the correction of the instrumental drift as determined empirically comparing the interpolated drift with the measured one from observations made with simultaneous wavelength calibration.

We used the SOPHIE automatic pipeline (Bouchy et al. 2009b) to extract the spectra from the detector images and to cross-correlate them with a G2-type mask derived from the Sun spectra. We obtained the radial velocities by fitting each resulting cross-correlation function (CCF) with a Gaussian (Baranne et al. 1996; Pepe et al. 2002). At this stage we rejected three spectra. Two of these spectra had a low *SNR* (*SNR*(550 nm) $\leqslant 30$), which rendered the correction for the CCD charge transfer inefficiency (CTI) less effective (Bouchy et al. 2009a). The third spectrum was contaminated by moonlight.

The final RV data set for HD 109246 comprises 58 measurements with a typical *SNR* of 47 (per pixel at 550 nm). This leads to a mean measurement uncertainty of 3.9 m s^{-1}, including photon noise and wavelength calibration errors. The photon-noise uncertainty was estimated as described in Appendix A. External systematic errors of 2 m s^{-1} (spectrograph drift uncertainty) and of 4 m s^{-1} (guiding errors) were quadratically added to the mean measurement uncertainty (Boisse et al. 2010a). The mean error bar on each RV measurement is then about 6 m s^{-1}. The RV measurements of HD 109246 are listed in Table C.1, available at the CDS. Table C.1 contains in its Cols. 1–3, the time of the observation (barycentric Julian date), the RV, and its error, respectively.

Table 1. Stellar parameters for HD 109246.

Parameters	Values
Sp. T.	G0V
m_V	8.77
$B - V$	0.64
π [mas]	15.24 ± 0.68
$T_{\rm eff}$ [K]	5844 ± 21^2
log g [cgs]	4.46 ± 0.19^2
Fe/H [dex]	0.10 ± 0.05^2
$v \sin i$ [km s^{-1}]	3 ± 1^1
M_* [$M_\odot$]	1.01 ± 0.11
R_* [$R_\odot$]	1.02 ± 0.07
$\log R'_{\rm HK}$ [dex]	-5.05 ± 0.1^2
Distance [pc]	65.6

Notes. (1) Parameter derived from the SOPHIE CCF (see Appendices). (2) Parameter derived from the SOPHIE spectra (see Appendices).

3. Stellar properties

HD 109246 (HIP 61177) is a G0 dwarf with an apparent V-band magnitude of $m_V = 8.77$ (SIMBAD database) and an astrometric parallax of $\pi = 15.14 \pm 0.68$ mas measured by Hipparcos (van Leeuwen 2007). Allende Prieto & Lambert (1999) derived a stellar mass $M_* = 1.01 \pm 0.11\ M_\odot$ and a radius $R_* = 1.02 \pm 0.07\ R_\odot$.

We determined the star's effective temperature, gravity, and metallicity using the spectroscopic analysis of Santos et al. (2004). This analysis was performed on the high-*SNR* average spectrum obtained by summing all the SOPHIE spectra. The spectroscopic analysis gave the following results: an effective temperature $T_{\rm eff} = 5844 \pm 21$ K, a surface gravity $\log g = 4.46 \pm 0.19$, a micro-turbulence velocity $V_{\rm t} = 1.01 \pm 0.02$ km s^{-1}, and a stellar metallicity [Fe/H] $= 0.10 \pm 0.05$ dex. When combined with isochrones (da Silva et al. 2006)[1], these parameters yield a stellar mass $M_* = 1.04 \pm 0.10\ M_\odot$, in agreement with the Allende Prieto & Lambert (1999) value. We also computed the projected rotational velocity and the stellar metallicity from the SOPHIE CCF as described in Appendix B. This gave $v \sin i = 3 \pm 1$ km s^{-1} and [Fe/H] $= 0.14 \pm 0.09$. This alternative estimation of the stellar metallicity is consistent with the accurate determination based on spectral analysis.

We estimated the stellar activity level from the emission in the core of the Ca II H&K bands measured on each spectra of HD 109246. The calibration used to derive $\log R'_{\rm HK}$ activity indexes from SOPHIE spectra is described in Appendix C. Applied to HD 109246, this calibration yields $\log R'_{\rm HK} = -5.05 \pm 0.1$, which translates into an RV dispersion that would be smaller than 1 m s^{-1} according to our experience on HARPS. The stellar parameters adopted for HD 109246 are listed in Table 1.

4. HD 109246b's orbital solution

4.1. Evidence for a planetary companion

As shown in Fig. 1, the RV data of HD 109246 exhibit a peak-to-peak variation of ~95 m s^{-1} and a dispersion of $\sigma_{\rm RV} = 28$ m s^{-1}. A clear signal with a semi-amplitude larger than 30 m s^{-1} is identified in the RV periodogram around 68 days. The dispersion of the bisector span values (BIS) is relatively low, with

[1] Web interface available on http://stev.oapd.inaf.it/cgi-bin/param

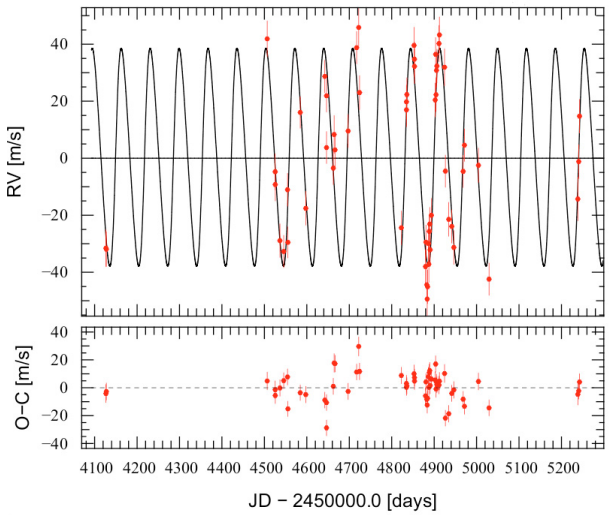

Fig. 1. Radial velocities (*top*) and residuals to the best-fit Keplerian model (*bottom*) for HD 109246 as a function of barycentric Julian date. The best-fit Keplerian model is represented by the black curve. The residuals have a dispersion of 10.2 m s^{-1}.

Table 2. Keplerian solution and inferred planetary parameters.

Parameters	Original velocities	Corrected velocities
$VR_{\rm mean}$ [km s^{-1}]	−19.463 ± 0.004	−19.464 ± 0.002
P [days]	68.20 ± 0.17	68.27 ± 0.13
K [m s^{-1}]	38.2 ± 2.2	38.2 ± 1.6
e	0.17 ± 0.07	0.12 ± 0.04
ω [deg]	273 ± 25	235 ± 29
T_0 [JD]	54 831.7 ± 4.2	54 824.6 ± 4.7
$M_{\rm P} \sin i$ [1] [$M_{\rm Jup}$]	0.76 ± 0.11	0.77 ± 0.09
a [1] [AU]	0.33 ± 0.09	0.33 ± 0.08
$\sigma_{\rm (O-C)}$ [m s^{-1}]	10.2	7.7

Notes. Results in the first column are based on the original RVs. Results in the second column are based on the corrected RVs (see text for details). [(1)] Assuming $M_* = 1.01 \pm 0.11\ M_\odot$.

$\sigma_{\rm BIS} = 9.9$ m s^{-1} (Fig. 2). No periodicity is detected in the bisector periodogram and no correlation is present in the bisector-RV plot (Fig. 2). All these observations support a scenario where the RV variations of HD 109246 are caused by the gravitational perturbation of an orbiting companion.

We fitted the RV data of HD 109246 with a Keplerian model using a Levenberg-Marquardt algorithm, after selected starting values with a genetic algorithm. The best solution is a mildly eccentric orbit ($e = 0.17 \pm 0.07$) with a period $P = 68.20 \pm 0.17$ days and a semi-amplitude $K = 38.2 \pm 2.2$ m s^{-1}. This signal corresponds to a planet of minimum mass $M_{\rm p} = 0.76 \pm 0.11\ M_{\rm Jup}$ orbiting HD 109246 with a semi-major axis of 0.33 ± 0.09 AU. The best-fit Keplerian model is plotted superimposed to the SOPHIE velocities in Fig. 1. The corresponding phase-folded RV curve is shown in Fig. 3 and the orbital elements of the planet are listed in Table 2. Uncertainties correspond to the 0.95 confidence interval after 5000 Monte-Carlo simulations. The tool used for the model fitting was successfully employed in exoplanetary surveys (e.g. Mayor et al. 2009; Bouchy et al. 2009b; Hébrard et al. 2009). The uncertainties in the minimum mass and in the semi-major axis take into account the uncertainties both in the stellar mass and in the signal semi-amplitude, period, and eccentricity.

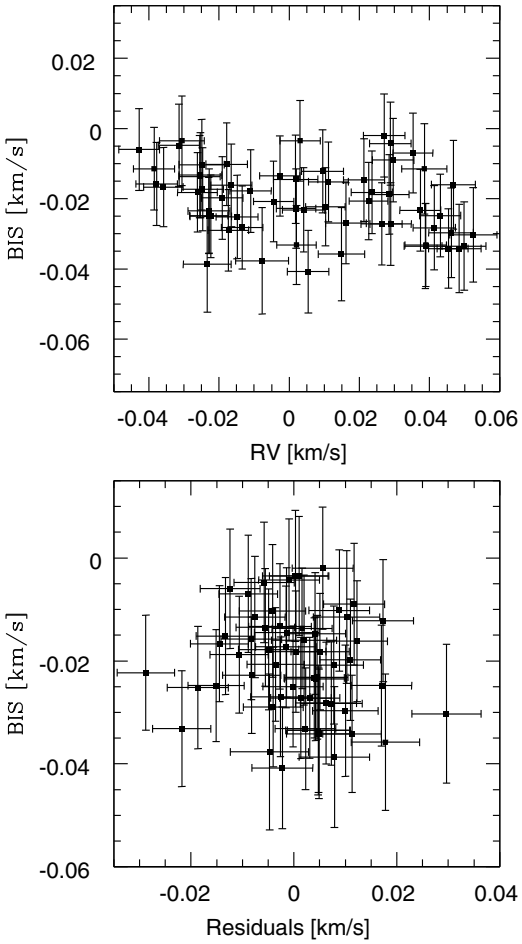

Fig. 2. Bisector span (BIS) as a function of RV (*top*), and as a function of the RV residuals (*bottom*). Uncertainties in the BIS are assumed to be twice the RV ones. In both panels the scale is the same in the x and y axes. No correlation is seen between BIS and RV residuals. The extra uncertainty seen in the RV data is unlikely to be caused by stellar activity.

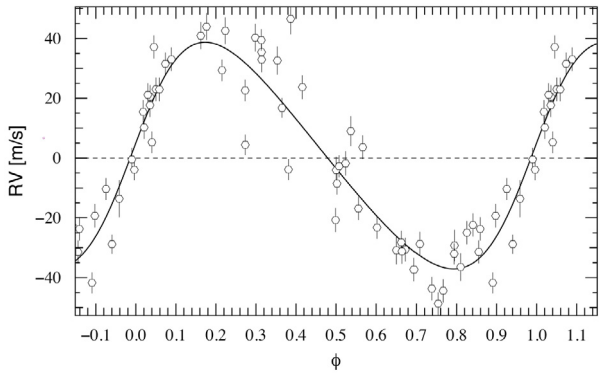

Fig. 3. Phase-folded RV curve for HD 109246. The solid line represents the Keplerian fit with a reduced χ^2 equal to 1.8. The period is 68.2 d, the eccentricity is 0.17, and the semi-amplitude is 38.2 m s^{-1}. Individual error bars are also plotted with a typical value of 6 m s^{-1}.

The residuals to the best-fit Keplerian model, $\sigma(O-C) = 10.2$ m s^{-1}, are a bit large compared to the mean error bar of ≈6 m s^{-1}. The reduced χ^2 is equal to 1.8, which suggests that an additional variation with a dispersion of ∼8 m s^{-1} is present in the data. If stellar jitter was the source of the excess variability

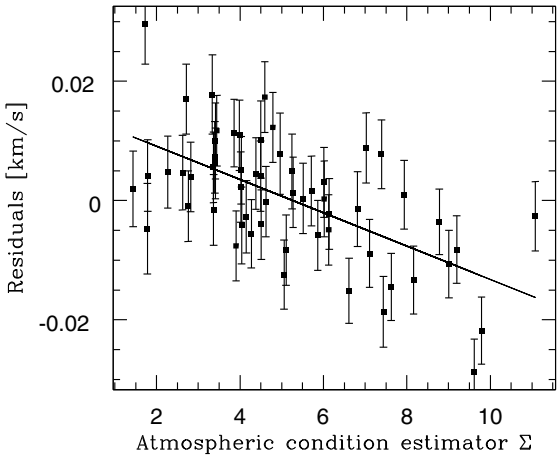

Fig. 4. Residuals to the Keplerian fit as a function of the atmospheric condition estimator Σ, inversely proportional to seeing (see Sect. 4.2 for the definition of Σ). The least-square fit represented by the solid line has a correlation coefficient of −0.6 and a Spearman coefficient of −0.56.

(in spite of an estimated value lower than 1 m s^{-1}, see Sect. 3), we could expect a negative correlation between the bisector span and the RV residuals (e.g. Queloz et al. 2001; Boisse et al. 2010b). As shown in Fig. 2, no such correlation is observed in the data. We note that the expected correlation would be very close to the detection limits but the level of activity needed to cause the RV variations is inconsistent with the $\log R'_{\rm HK}$ value.

About a quarter of gaseous giant planet are in a multiple planetary system. The excess variability may thus alternatively be due to the presence of an additional planet in the system. We did not find any indication for a second planet in the present data set. With a maximum semi-amplitude of 14 m s^{-1}, the RV residuals exclude the presence of an inner planet with $m_{\rm p} \sin i \geqslant 0.28\ M_{\rm Jup}$. A longer period planet could not induce a linear drift larger than 0.4 m s^{-1}. Additional data will be needed to probe the presence of low-mass inner planets and to constrain the presence of possible outer companions.

The third and best possible explanation to the relatively large RV residuals is the underestimation of an instrumental effect. Described in the next section, the so-called seeing effect seems to affect the observations of HD 109246 (Fig. 4).

4.2. Spectrograph illumination limitation

The large residuals of HD 109246 RVs to the best-fit Keplerian model seem well explained by seeing effect due to bad scrambling of one multimode fiber (Fig. 4). This effect was presented in details in Boisse et al. (2010a). We summarize here the main issue for the SOPHIE HR mode.

SOPHIE is a fiber-fed spectrograph. The stellar light collected by the telescope is led to the instrument through a standard step-index multi-mode cylindrical optical fiber. They have good azimuthal scrambling but the radial one is not perfect. In order to improve the scrambling ability of the fiber and to stabilize the illumination, optical double scrambler are usually coupled to the fibers (as it is done for the SOPHIE HR mode) (Brown 1990; Hunter & Ramsey 1992). Non-uniform illumination of the slit or output fiber at the spectrograph entrance (variations in seeing, focus, and image shape) decreases the RV precision, owing to non-uniform illumination inside the pupil of the spectrograph that leads, with optical aberrations to variation in the centroids of the stellar lines on the focal plane.

Our experience on SOPHIE has led to identify remaining RV limitations due to the incomplete fiber scrambling. We simulated the optical path in the SOPHIE spectrograph and observed that variations of the slit, pupil or optical fiber illumination are directly translated on the spectrum. The displacement of the spectrum on the CCD detector is a function of wavelength (or position on the detector) and is proportional to the width of the input image at the entrance of the fiber. Because the effect is not symmetric along the spectral orders and not monitored by the calibration lamp, the final computed RV varies and its variation is proportional to the input image width.

The value of the seeing is not monitored by SOPHIE up until recently. We estimated the atmospheric condition by calculating the relative flux by unit of exposure time:

$$\Sigma = \frac{SNR^2}{T_{\rm exp} 10^{-M_{\rm V}/2.5}}, \text{ or for the same star } \Sigma = \frac{SNR^2}{T_{\rm exp}} \quad (1)$$

with $T_{\rm exp}$ the exposure time of the measurement and $M_{\rm V}$ the visual magnitude of the target. This parameter allows a relative estimation of the seeing since we cannot evaluate the atmospheric absorption. The atmospheric condition estimator Σ is inversely proportional to the seeing value.

The seeing effect is expected to affect the measurements since the input beam at the entrance of SOPHIE is center-illuminated (input image smaller than the 3″ sky acceptance of the optical fiber). In this case, simulations predict a systematic decrease in measured RV values, which is observed in the obtained data, as shown in Fig. 4 of this paper and for a sample of SOPHIE targets in Fig. 5 from Boisse et al. (2010a). Moreover, when the input image is smaller than the diameter of the fiber, we are more sensitive to effect of guiding and centering system that introduce RV variations. These RV variations are quite random and add some noise, whereas the seeing effect is directly related to the optical path in the spectrograph and may be quantified. We are modeling these variations with our data in order to remove this noise with a software tool even if this correction is only relative because of our inability to estimate the absorption parameter. The seeing effect may reach peak-to-peak RV variations of 20 m s^{-1} and it is the main current limitation of the SOPHIE accuracy. A new guiding camera is now in operation on SOPHIE and allows a better guiding and centering, and also a monitoring of the exact seeing. It will then allow us to refine this method of correction. Tests on square and octagonal section fibers to optimize the fibers scrambling are now under development and SOPHIE will be used as a bench test to validate these new feed optics. Soon, a new double scrambler will be mounted on SOPHIE with the goal to reduce this effect by at least a factor 10.

4.3. Corrected velocities and improved orbital solution

In Fig. 4, the residuals to the Keplerian fit are correlated with the atmospheric condition estimator Σ (see Eq. (1)). We calculate the linear correlation coefficient that is equal to −0.6 and the Spearman coefficient equal to −0.56, which support the anti-correlation between the two parameters. The linear function determined by a least-squares fit was subtracted from the RV data measurements to correct for the seeing effect. Fitting a Keplerian model to the corrected RVs yields the orbital parameters reported in the right column of Table 3. The new planetary orbit is similar to the previous one; the major change introduced by the correction is to decrease the RV residuals to 7.7 m s^{-1}. This new value

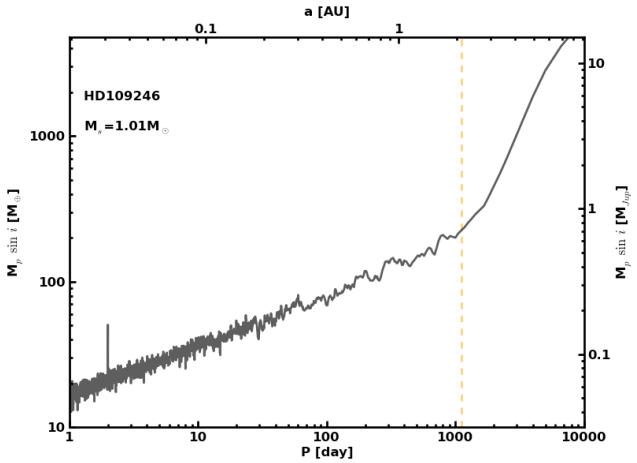

Fig. 5. Mass limit exclusion diagram with 99% confidence level for an additional companion in the HD 109246 system calculated from the residuals after the best-fit Keplerian model on the corrected velocities. The dashed line corresponds to the observation span. The two days peak expresses the lower efficiency at this period due to data sampling.

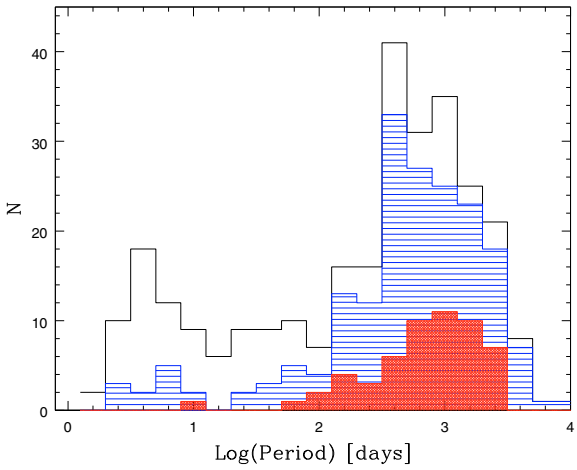

Fig. 6. Period distribution of the known extrasolar planet orbiting single dwarf stars discovered via RV surveys. With a period of 68 days, HD 109246b is in the middle of the "period valley". Horizontal stripped illustrates the distribution for planets more massive than 0.8 $M_{\rm Jup}$ and the shaded one for planets more massive than 4 $M_{\rm Jup}$.

does not change a lot our previous conclusions regarding the possible presence of an additional planet as illustrated in Fig. 5. The remaining variability excess might be accounted for by an increase in guiding and centering errors when the input image is smaller than the fiber diameter (see Sect. 4.2) or by RV jitter owing to stellar activity (see Sect. 3).

5. Discussion and conclusion

We report the detection of an extrasolar planet candidate around HD 109246 discovered with the SOPHIE spectrograph mounted on the 1.93-m telescope at the Haute-Provence Observatory. HD 109246b is characterized by a minimum mass of 0.77 ± 0.09 $M_{\rm Jup}$, an orbital period of 68.27 ± 0.13 days, and an eccentricity of 0.12 ± 0.04. The host star being slightly more metallic than the Sun, the discovery of HD 109246b reinforces the correlation between giant planet occurrence and stellar metallicity (e.g., Santos et al. 2004, 2005; Fischer & Valenti 2005). No photometric search for transits have been undertaken until now though the transit probability is slightly above 1%.

The residuals to the single-planet Keplerian fit (10.2 m s^{-1}) are larger than the mean error bar of ≈6 m s^{-1}, which suggests the presence of an additional source of RV variability. We considered three possibilities: stellar jitter, the presence of an additional planet in the system, and an instrumental effect related to seeing variations. We did not detect a clear signature of stellar activity, nor that of an additional planet. On the other hand, we identified a correlation between the residuals to the Keplerian fit and a seeing indicator. Correcting the RVs of HD 109246 for this systematic effect decreased the RV residuals to 7.7 m s^{-1} while preserving the original planetary orbit. This result indicates that the seeing effect described in Boisse et al. (2010a) is at least partly responsible for the excess variability measured in the velocities of HD 109246. A new guiding camera is now in operation on the 1.93-m telescope at OHP. Besides providing better guiding and centering performances, this new camera allows for a direct monitoring of the seeing. Future observations shall thus allow the method described in this paper to correct SOPHIE data for the seeing effect to be refined. Moreover, a new double scrambler will be mounted on SOPHIE to improve the scrambling ability of the fibers and remove the seeing effect.

The most remarkable property of HD 109246b is that its orbital parameters place it within the so-called "period valley" in the period distribution of extrasolar planets (Fig. 6). The period valley extends from ∼10 to ∼100 days (Udry et al. 2003). It separates the pile-up of hot Jupiters from the population of giant planets with periods above ∼1 year. HD 109246b mass reinforces the fact that light planets ($m_{\rm p} \sin i \leqslant 0.8\ M_{\rm Jup}$) are preferentially found to orbit with short period ($P \leqslant 100$ d) (Udry & Santos 2007). Ignoring multiple stars systems, RV surveys do not detect massive planets with $m_{\rm p} \sin i \geqslant 4\ M_{\rm Jup}$ with period less than 100 days. The two components left are HD 162 020b, a probable brown dwarf (Udry et al. 2002) and one of the two massive components orbiting HD 168 443 (Marcy et al. 2001; Udry et al. 2002). Including the transit surveys detections, planets more massive than 4 $M_{\rm Jup}$ are not found in the "period valley".

A comparison with the models of Mordasini et al. (2009) shows that HD 109246b may belong to the population of "main clump" planets. If so, it probably started to form near 4–6 AU and then moved inwards through type II migration. As outlined by Mordasini et al. (2009), the number of giant planets orbiting inside 1 AU is an important observational parameter for planet formation models. Additional detections of planets like HD 109246b will thus help characterize the profile of the surface density of solids below 1 AU and the efficiency with which migrating cores can accrete planetesimals.

Acknowledgements. The authors thanks all the staff of Haute-Provence Observatory for their contribution to the success of the SOPHIE project and their support at the 1.93-m telescope. We wish to thank the "Programme National de Planétologie" (PNP) of CNRS/INSU, the Swiss National Science Foundation, and the French National Research Agency (ANR-08-JCJC-0102-01 and ANR-NT05-4-44463) for their continuous support to our planet-search programs. A.E. is supported by a fellowship for advanced researchers from the Swiss National Science Foundation (grant PA00P2_126150/1). N.C.S. would like to thank the support by the European Research Council/European Community under the FP7 through a Starting Grant, as well from Fundação para a Ciência e a Tecnologia (FCT), Portugal, through a Ciência 2007 contract funded by FCT/MCTES (Portugal) and POPH/FSE (EC), and in the form of grants reference PTDC/CTE-AST/098528/2008 and PTDC/CTE-AST/098604/2008. D.E. is supported by CNES. This research has made use of the SIMBAD database and the VizieR catalogue access tool operated at CDS, France. The authors thanks the referee for his careful reading and judicious remarks.

Appendix A: Determination of the RV uncertainty from the SOPHIE Cross-Correlation Function

The methodology to compute the photon-noise uncertainty of RV measurement was described by Bouchy et al. (2001). In this approach, the quality factor Q represents the instrinsic RV-information content of a given spectrum (quality and richness of spectral lines). This Q factor is independent of the flux and is computed on a reference spectrum considered as noise free. The RV uncertainty $\delta V_{\rm rms}$ is then computed using the following relation:

$$\delta V_{\rm rms} = \frac{c}{Q\ \sqrt{N_{\rm e^-}}}, \tag{A.1}$$

with c the speed of light and $N_{\rm e^-}$ the total number of photoelectrons counted over the whole spectral range. In practice one does not always have a noise free reference spectra and one needs to estimate correctly the RV uncertainty on real observed spectra. On a noisy spectrum, the high frequency structures due to noise increase artificially the Q factor and lead to an underestimated uncertainty for the RV. We estimate that the computation of the Q factor is correct for spectra with *SNR* per pixel higher than ∼200. For lower *SNR*, Q is overestimated and $\delta V_{\rm rms}$ is therefore underestimated.

We adapted our methodology directly to the CCF which corresponds to an average spectral line in velocity space at much higher *SNR* than individual lines and may be considered as noise free for the computation of the quality factor. In that case Q_{CCF} can be expressed by the relation:

$$Q_{CCF} = \frac{\sqrt{\sum_i \left(\frac{\partial CCF(i)}{\partial V(i)}\right)^2 / CCF^2_{\rm noise}(i)}}{\sqrt{\sum_i CCF(i)}} \cdot \sqrt{N_{\rm scale}}, \tag{A.2}$$

where $CCF(i)$ is the Cross-Correlation Function measured for the velocity i, and $CCF_{\rm noise}(i)$ is the quadratic sum of the photon noise and the detector noise integrated inside the CCF mask holes for the velocity i. The correction factor $N_{\rm scale}$ corresponds to the scale of the velocity step in detector pixel unit. The RV uncertainty $\delta V_{\rm rms}$ is then equal to:

$$\delta V_{\rm rms} = \frac{1}{Q_{CCF}\ \sqrt{\sum CCF(i)}}. \tag{A.3}$$

This RV uncertainty, directly computed on the CCF, is robust and can be applied to any kind of spectra down to *SNR* of ∼20. Figure A.1 shows the RV uncertainty scaled to an equivalent *SNR* of 100 and computed for a sub-sample of our planet search program with SOPHIE in HR mode. The RV uncertainty is plotted versus the index $B-V$, and for two classes of $v \sin i$ ($\leqslant$3 km s^{-1} and in between 6 and 10 km s^{-1}). It illustrates the dependence with the effective temperature and the projected rotational velocity of the stars.

Appendix B: Determination of *v* sin *i* and [Fe/H] from the SOPHIE Cross-Correlation Function

We used the property that the CCF can be considered as an average line of the target spectrum. Line profiles are directly related to the stellar atmospheric parameters (e.g. abundances, thermal expansion), macro and micro-turbulence, rotation rate, and instrumental profile. Then, stellar properties affect spectral lines included in the correlation mask and are reflected in the CCF. We can derive stellar properties in analyzing the *FWHM* and the contrast of the fitted Gaussian on the SOPHIE CCF. The $v \sin i$ of a star might be derived as described by Benz & Mayor (1981) for the CORAVEL spectrograph. They refined their calibration afterward (Benz & Mayor 1984). Queloz et al. (1998a) applied it to the ELODIE spectrograph. The stellar [Fe/H] calibration was first done by Mayor (1980) for the CORAVEL CCF, improved by Pont (1997). The both calibrations is done here for the SOPHIE spectrograph following the Santos et al. (2002) methodology for the CORALIE spectrograph. The spectral line profile is dependent of the instrumental one, so these calibrations had to be derived for different instruments.

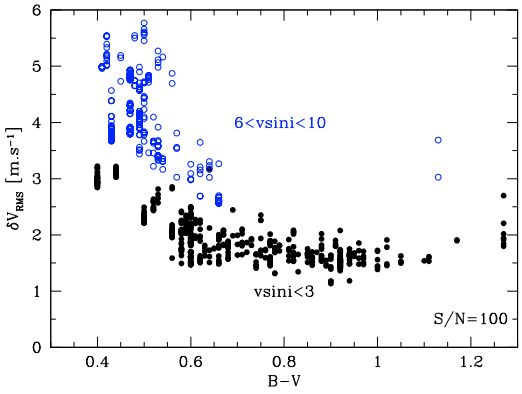

Fig. A.1. RV uncertainty versus the index $B-V$, and for two classes of $v \sin i$, $\leqslant$3 km s^{-1} (plain dark circles) and in between 6 and 10 km s^{-1} (open blue circles), for SOPHIE observations in high-resolution mode with *SNR* of 100.

B.1. Calibration of the projected rotational velocity v sin i

We calibrated the relation between the $v \sin i$ and the width σ of the CCF for both observing modes, high-efficiency (HE) and high-resolution (HR), of SOPHIE spectrograph using the cross-correlation masks G2 and K5 which have almost the same CCF width (negligible at the photon noise level). We note that the metallicity does not affect too much the width of the lines in comparison with the expected precision of our calibration. For solar-type stars, these two variables can be related by:

$$v \sin i = A \cdot \sqrt{\sigma^2 - \sigma_0^2} \tag{B.1}$$

where σ represents the measured Gaussian width of the CCF ($FWHM/2\sqrt{2\ln 2}$), σ_0 the value of the expected σ for a "non-rotator" of a given spectral type, and A is a constant relating the "excess" width of lines to the actual projected rotational velocity $v \sin i$.

We first determine the quantity σ_0 by adjusting the lower envelope of the distribution of points in the diagram, shown in Fig. B.1 for HR mode, of σ versus $B-V$ which is quite well related with stellar temperature for dwarfs with $B-V$ index in the range 0.4–1.3. We neglected here the effect of the metallicity. The adjusted lower envelopes for HR and HE mode are well described by:

$$\sigma_{0\_\rm HR} = 9.90 - 22.56(B-V) + 22.37(B-V)^2 - 6.95(B-V)^3 \tag{B.2}$$

$$\sigma_{0\_\rm HE} = 10.52 - 22.56(B-V) + 22.37(B-V)^2 - 6.95(B-V)^3. \tag{B.3}$$

The other variable in Eq. (B.1) we need to determine is A, i.e., the constant relating the $v \sin i$ to the excess width of the CCF.

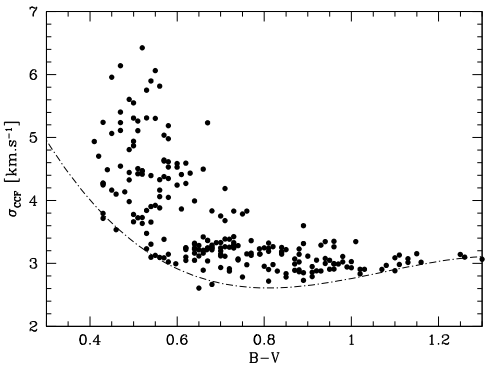

Fig. B.1. Gaussian width of the SOPHIE CCF versus $B-V$ index for 240 dwarf stars observed in HR mode. The lower envelope determines the locus of "non-rotator" stars.

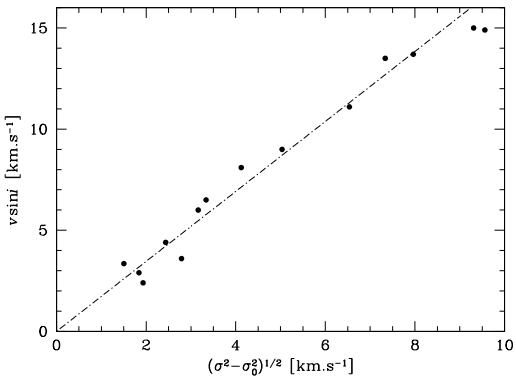

Fig. B.2. Known $v \sin i$ versus measured σ in the HR mode and the adjusted slope.

For that we observed with SOPHIE 14 stars with known $v \sin i$ from the catalog of rotational velocities of F and G stars (Reiners & Schmitt 2003), and we find $A = 1.73$ and $A = 1.64$ for respectively HR and HE mode. Figure B.2 shows the relation obtained between the known $v \sin i$ and the measured σ for the HR mode. We note that this relation is valid up to $v \sin i = 20$ km s^{-1} (Bouvier, private communication). The estimated uncertainty on $v \sin i$ is 1 km s^{-1}.

We find only three values of $v \sin i$ from known planet hosting stars: HD 189733 and HD 80606 from Butler et al. (2006), and HD 17156 from Fischer et al. (2007) with spectroscopic determination that may have its own uncertainty. Their estimations for these stars are about 1.5 km s^{-1} above our estimate. On the other hand, our calibration find a value of 2.6 km s^{-1} for the Sun $v \sin i$. These values are satisfactory for the precision required.

The technique described above represents a simple way of obtaining an estimation of projected rotational velocities for dwarfs, simply as a by-product of the precise RV measurements. In particular, this calibration permits us to obtain quite easily values for the $v \sin i$ for all the stars in the SOPHIE exoplanet search program.

B.2. Calibration of the metallicity

The different SOPHIE masks are mainly built with neutral weak lines. An important quantity of ferric ions increases the absorption coefficient for the lines of these elements. The lines then become deeper and the contrast of the CCF larger. But, the line contrast depends also on the spectral type, measured by the $B-V$

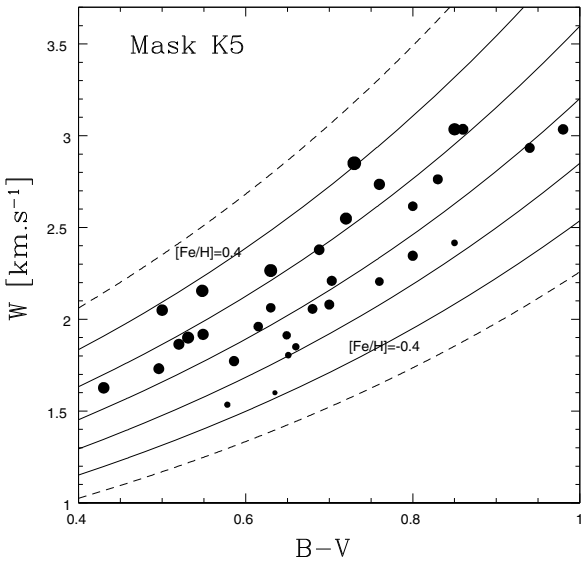

Fig. B.3. Surface of the CCF, W, as a function of the $B-V$ for the K5 correlation mask. The dot size is proportional to the spectroscopic metallicity. The solid lines draw the relationship between the parameters for [Fe/H] = const. The fit with an exponential is good in the domain of metallicity but it is obviously wrong for $B-V \geqslant 1.0$.

for a same luminosity class. The higher is the $B-V$, the lower is the effective temperature and the spectrum has more lines of metallic atoms. In addition, stellar rotation and Doppler shift, related to the relative speed of each atoms, modify the shape of the CCF widening and spreading the line profile but, it does not change the line surface. To take into account the stellar rotation and the macroturbulence at the stellar surface, we computed the total area W of the Gaussian in spite of CCF contrast, $W = \sqrt{2\pi}$ (contrast/100)σ where σ represents the measured Gaussian width of the CCF and the contrast is expressed in percentage, and studied its dependence as a function of the $B-V$ and metallicity. It is expected that the CCF surface grows with metallicity and with the $B-V$.

A unique independent measurements of the metallicity has to be done for the calibration. We used a spectroscopic analysis based on a detailed study of each line (Santos et al. 2004). We determined accurately the [Fe/H] of 32 targets covering the $B-V$ and CCF surface domains. The mean uncertainty from the spectroscopic determination is about 0.1 dex.

SOPHIE has two modes of observations (Bouchy et al. 2009b), the HR and the HE mode. Two fibers are used for each mode: one for the star and the other for the sky spectrum or for simultaneous calibration lamp exposure. The CCF surface is independent of the observation mode, provided that the *SNR* is sufficient (i.e. $SNR \geqslant 20$ or $SNR \geqslant 100$ for thorium simultaneous mode which produces an important background of scattered light all over the CCD). On the other hand, the CCF contrast, and so the CCF surface, depends on the calibration mask used. We studied SOPHIE masks of spectral type G2 and K5 because the calibration is limited in $B-V$, excluding the coldest and the warmest stars. For the K5 mask, the fit, shown in Fig. B.3, gives:

$$[\mathrm{Fe/H}] = 0.2615 + 3.9553 \log W - 2.2606(B-V). \quad \text{(B.4)}$$

Samely, for the G2 mask, we obtained:

$$[\mathrm{Fe/H}] = -0.9440 + 3.8807 \log W - 1.4992(B-V). \quad \text{(B.5)}$$

These calibrations are valid for $0.43 \leqslant (B-V) \leqslant 0.98$ and $-0.47 \leqslant [\mathrm{Fe/H}] \leqslant 0.44$.

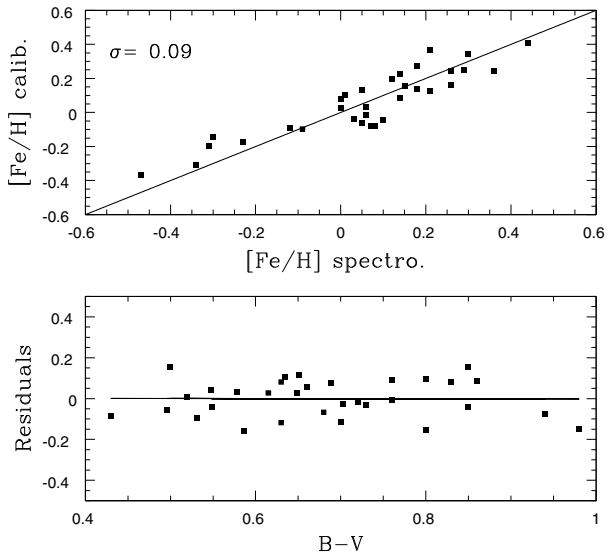

Fig. B.4. *Top*: [Fe/H] computed from the calibration as a function of the spectroscopic estimation. The solid line illustrates a 1:1 correlation. *Bottom*: residuals from the calibration as a function of the $B - V$.

We compare the [Fe/H] values obtained from the CCF surface and from the spectroscopic analysis in Fig. B.4. The dispersion of the residuals around the zero values is 0.09 dex which is satisfactory given the spectroscopic uncertainty. We do not observe any trend with the stellar temperature or $B - V$ as shown in Fig. B.4. Our calibration is in agreement with others spectroscopic determination of the metallicity: Sousa et al. (2006), Sousa et al. (2008), Gonzalez et al. (2007), and Fischer & Valenti (2005) as shown in Fig. B.5.

The tool included in the SOPHIE data reduction software allows an immediate estimation of the [Fe/H] of the star with a good approximation (±0.09 dex). Our aim is to have a quick estimate of the target metallicity to focus our planet-search survey around over-metallic stars. One goal of the program is to find new hot-Jupiters known to be more prevalent around metal-rich stars (e.g., Santos et al. 2004, 2005).

Appendix C: Determination of log R'_{HK} from the SOPHIE spectra

The SOPHIE spectra, with a bandpass from about 3900 Å to 6800 Å, include both Calcium II H and K resonant lines centered at 3968.49 Å and 3933.68 Å respectively. These lines are widely used indicators of stellar magnetic activity. In Fig. C.1 are plotted two high-*SNR* SOPHIE spectra of the Ca II lines central region for the chromospherically active star HD 131156 and the inactive HD 187013. An active star for which spots and plages are present on the photosphere is characterized by an emission in the center of the absorption line (e.g. Boisse et al. 2009).

The stellar activity is parametrized by an index created by Wilson (1968) defined by the ratio between the emitted flux in the center of the lines and the continuum flux. The S-value is defined by the measure of the quotient of the flux in two triangular bandpasses centered on the H and K emission cores and two continuum regions on either side. We define our Ca II H&K index following the Mt. Wilson S_{MW} index (Baliunas et al. 1995; Boisse et al. 2009):

$$\text{Index} = \frac{H + K}{B + V} \tag{C.1}$$

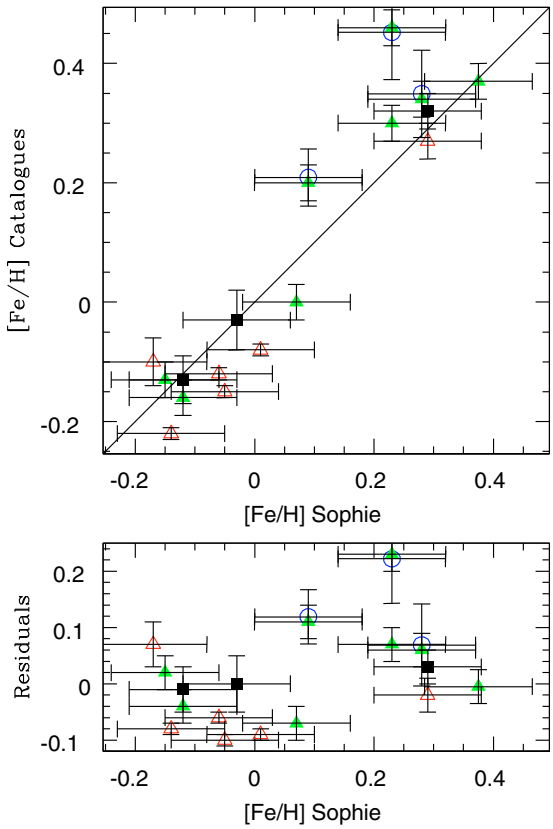

Fig. B.5. *Top*: [Fe/H] from others estimations from spectroscopic analyses: Sousa et al. (2006) (black squares), Sousa et al. (2008) (red open triangles), Gonzalez et al. (2007) (blue circle), and Fischer & Valenti (2005) (filled green triangles) as function of those from SOPHIE calibration. The solid line illustrates a 1:1 correlation. *Bottom*: residuals from the top panel as a function of [Fe/H] from SOPHIE calibration. The rms of the residuals is 0.09 dex.

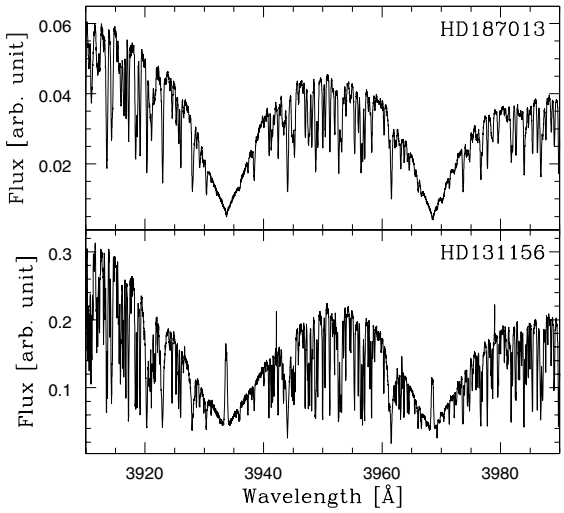

Fig. C.1. Two SOPHIE spectra of the region of the CaII H and K lines between 3900 and 4000 Å. *Top*: non active star. *Bottom*: active star.

where H and K are the flux measured in the triangular 1.09 Å *FWHM* window centered on each line of the Ca II doublet, and B and V estimate the continuum on both sides with the flux measured in 20 Å wide windows respectively centered on 3900 Å and 4000 Å. An automatic cut of the cosmic rays are done. Each

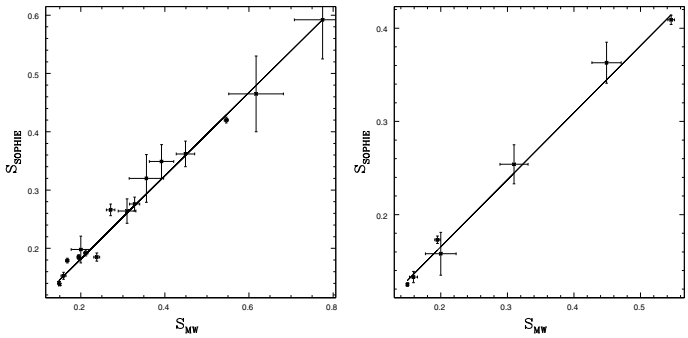

Fig. C.2. Mean $S_{\rm SOPHIE}$ values as a function of the Mount Wilson values from Duncan et al. (1991). The solid line is the best-linear fit to the data. *Left*: HR mode. (rms = 0.012) *Right*: HE mode. (rms = 0.007).

line is located in two consecutive orders of the SOPHIE spectra. For the K line, we average the flux measured in two orders. As one of the H line is located on the edge of the an order where less flux is collected which introduce noise, only the flux measured in the H line of another order is kept.

When studying the Ca II H&K lines in SOPHIE spectra, one must account for the fact that they are located in a spectral region that suffers from contamination from background scattered light. In order to use the signature of flux emitted in the Ca II lines, we estimate a background light level and subtract it from the stellar spectra. For each mode, two fibers are used on SOPHIE, one of which is pointed on the target. The other fiber receives the sky spectrum or is fed with a Thorium-Argon lamp. The background light level of a stellar order is estimated from the same order of the other fiber by fitted a polynomial function on local minima. We put limits on the minimal *SNR* in the first order ($\lambda \sim 3955$ Å) where both Ca II H&K lines are found to have a good estimation of the activity index. The boundaries are fixed where dependency between *SNR* and $\log R'_{\rm HK}$ is no longer observed. If the second aperture received the sky spectrum, the background light level is low and the minimal *SNR* is equal to 10. When the Thorium-Argon lamp feed the second fiber, the level of background light on the CCD is about 0.1% of the stellar continuum and the minimal *SNR* to have a reliable value of $\log R'_{\rm HK}$ is fixed at 30.

We measure a chromospheric index $S_{\rm SOPHIE}$ that is calibrated to the Mount Wilson index $S_{\rm MW}$ by observing calibration stars in HE and HR SOPHIE mode. The Mount Wilson values from Duncan et al. (1991) and our measurements $S_{\rm SOPHIE}$ are listed in Table C.2, available in the electronic form of the paper. Table C.2 contains in its Cols. 1–6, the name of the stars, the $S_{\rm MW}$ value, and its error, the $S_{\rm SOPHIE}$, and its error, and the SOPHIE observational mode, respectively. The mean $S_{\rm SOPHIE}$ values compared with $S_{\rm MW}$ are shown in Fig. C.2 for the set of calibrating stars for both mode of SOPHIE. In HR mode, the best linear fit to the data gives:

$$S_{\rm SOPHIE} = (0.71 \pm 0.03) S_{\rm MW} + (0.039 \pm 0.006). \quad \text{(C.2)}$$

In HE mode, the relation is:

$$S_{\rm SOPHIE} = (0.72 \pm 0.02) S_{\rm MW} + (0.021 \pm 0.006). \quad \text{(C.3)}$$

With this index, we can calculate the litterature's index corrected from photospheric emission, $R'_{\rm HK}$ (Noyes et al. 1984). This measure is available only for $0.43 \leqslant (B-V) \leqslant 1.2$.

We estimate the uncertainty of our index (±0.1 dex) with the dispersion on our values for a same star over one year. This dispersion may be due to intrinsic variations of the stellar activity. But, we consider that our main error comes from the subtraction of the background light.

References

Albrecht, S., Reffert, S., Snellen, I. A. G., & Winn, J. N. 2009, Nature, 461, 373
Allende Prieto, C., & Lambert, D. L. 1999, A&A, 352, 555
Baliunas, S. L., Donahue, R. A., Soon, W. H., et al. 1995, ApJ, 438, 269
Bakos, G. A., Shporer, A., Pal, A., et al. 2007, ApJ, 671, L173
Baranne, A., Queloz, D., Mayor, M., et al. 1994, A&AS, 119, 373
Benz, W., & Mayor, M. 1981, A&A, 93, 235
Benz, W., & Mayor, M. 1984, A&A, 138, 183
Boisse, I., Moutou, C., Vidal-Madjar, A., et al. 2009, A&A, 495, 959
Boisse, I., Bouchy, F., Chazelas, B., et al. 2010a, in New technologies for probing the diversity of brown dwarfs and exoplanets, EPJ Web of Conferences, in press [arXiv:1001.0794]
Boisse, I., Bouchy, F., Hébrard, G., et al. 2010b, A&A, submitted
Bouchy, F., Pepe, F., & Queloz, D. 2001, A&A, 374, 733
Bouchy, F., Pont, F., Melo, C., et al. 2005, A&A, 431, 1105
Bouchy, F., Queloz, D., Deleuil, M., et al. 2008, A&A, 482, 25
Bouchy, F., Isambert, J., Lovis, C., et al. 2009a, in Astrophysics Detector Workshop, EAS publication, ed. P. Kern, in press
Bouchy, F., Hébrard, G., Udry, S., et al. 2009b, A&A, 505, 853
Brown, T. M. 1990, ASPC, 8, 335
Butler, R. P., Wright, J. T., Marcy, G. W., et al. 2006, ApJ, 646, 505
Cameron, A. C., Bouchy, F., Hébrard, G., et al. 2007, MNRAS, 375, 951
da Silva, L., Girardi, L., Pasquini, L., et al. 2006, A&A, 458, 609
Da Silva, R., Udry, S., Bouchy, F., et al. 2006, A&A, 446, 717
Delfosse, X., Forveille, T., Perrier, C., & Mayor, M. 1998, A&A, 331, 581
Duncan, D. K., Vaughan, A. H., Wilson, O. C., et al. 1991, ApJ, 76, 383
Fischer, D. A., & Valenti, J. 2005, ApJ, 622, 1102
Fischer, D. A., Vogt, S. S., Marcy, G. W., et al. 2007, ApJ, 669, 1336
Galland, F., Lagrange, A. M., Udry, S., et al. 2005, A&A, 444, L21
Gonzalez, G., & Laws, C. 2007, MNRAS, 378, 1141
Hébrard, G., Bouchy, F., Pont, F., et al. 2008, A&A, 481, 52
Hébrard, G., Bonfils, X., Ségransan, D., et al. 2010a, A&A, 513, A69
Hébrard, G., Désert, J.-M., Díaz, R., et al. 2010b, A&A, 516, A95
Hunter, T. D., & Ramsey, L. W. 1992, PASP, 104, 1244
Marcy, G. W., Butler, R. P., Vogt, S. S., et al. 2001, ApJ, 555, 418
Mayor, M. 1980, A&A, 87, L1
Mayor, M., & Queloz, D. 1995, Nature, 378, 355
Mayor, M., Bonfils, X., Forveille, T., et al. 2009, A&A, 507, 487
Mordasini, C., Alibert, Y., Benz, W., & Naef, D. 2009, A&A, 501, 1161
Mosser, B., Bouchy, F., Martić, M., et al. 2008, A&A, 478, 197
Moutou, C., Hébrard, G., Bouchy, F., et al. 2009, A&A, 498, L5
Naef, D., Mayor, M., Beuzit, J. L., et al. 2005, in Stellar Systems and the Sun, Proceedings of the 13th Cambridge Workshop on Cool Stars, ed. F. Favata, et al., ESA, SP-560, 833
Noyes, R. W., Hartmann, L. W., Baliunas, S. L., Duncan, D. K., & Vaughan, A. H. 1984, ApJ, 279, 763
Ohta, Y., Taruya, A., & Suto, Y. 2005, ApJ, 622, 1118
Pepe, F., Mayor, M., Galland, F., et al. 2002, A&A, 388, 632
Perrier, C., SIvan, J. P., Naef, D., et al. 2003, A&A, 410, 1039
Perruchot, S., Kohler, D., Bouchy, F., et al. 2008, in Ground-based and Airborn Instrumentation for Astronomy II, ed. I. S. McLean, & M. M. Casali, Proc. SPIE, 7014, 7014J
Pont, F. 1997, Ph.D. Thesis, Geneva University
Pont, F., Hébrard, G., Irwin, J. M., et al. 2009, A&A, 509, 695
Queloz, D., Allain, S., Mermilliod, J.-C., et al. 1998a, A&A, 335, 183
Queloz, D., Mayor, M., Sivan, J. P., et al. 1998b, in Brown dwarfs and extrasolar planets, ed. R. Rebolo, E. L. Martin, & M. R. Z. Osorio, ASP Conf. Ser., 134, 324
Queloz, D., Eggenberger, A., Mayor, M., et al. 2000, A&A, 359, 13
Queloz, D., Henry, G. W., Sivan, J. P., et al. 2001, A&A, 379, 279
Reiners, A., & Schmitt, J. H. M. M. 2003, A&A, 398, 647
Santos, N. C., Mayor, M., Naef, D., et al. 2000, A&A, 361, 265
Santos, N. C., Israelian, G., & Mayor, M. 2001, A&A, 373, 1019
Santos, N. C., Mayor, M., Naef, D., et al. 2002, A&A, 392, 215
Santos, N. C., Israelian, G., & Mayor, M. 2004, A&A, 415, 1153
Santos, N. C., Israelian, G., Mayor, M., et al. 2005, A&A, 493, 639
Sousa, S. G., Santos, N. C., Israelian, G., et al. 2006, A&A, 458, 873
Sousa, S. G., Santos, N. C., Mayor, M., et al. 2008, A&A, 487, 373
Triaud, A. H. M. J., Collier Cameron, A., Queloz, D., et al. 2010, A&A, accepted
Udry, S., & Santos, N. C. 2007, ARA&A, 45, 397
Udry, S., Mayor, M., Naef, D., et al. 2002, A&A, 390, 267
Udry, S., Mayor, M., & Santos, N. C. 2003, A&A, 407, 369
Udry, S., Mayor, M., Benz, W., et al. 2006, A&A, 447, 361
van Leeuwen, F. 2007, A&A, 474, 653
Vaughan, A. H., & Preston, G. W. 1980, PASP, 92, 385
Wilson, O. C. 1968, ApJ, 153, 221
Winn, J. N. 2010 [arXiv:1001.2010]